Bioconjugate Chemistry

pubs.acs.org/bc Article

Prostate-Specific Membrane Antigen-Targeted Turn-on Probe for Imaging Cargo Release in Prostate Cancer Cells

Feyisola P. Olatunji, Emily A. Savoy, Mylan Panteah, Nooshin Mesbahi, Armina Abbasi, Cresencia M. Talley, Christine L. Lovingier, Leslie A. Caromile,* and Clifford E. Berkman*

Cite This: *Bioconjugate Chem.* 2021, 32, 2386−2396 Read Online

ACCESS | Metrics & More | Article Recommendations | Supporting Information

ABSTRACT: The tunable nature of phosphoramidate linkers enables broad applicability as pH-triggered controlled-release platforms, particularly in the context of antibody- and small-molecule-drug conjugates (ADCs and SMDCs), where there remains a need for new linker technology. Herein, we explored in-depth the release of turn-on fluorogenic payloads from a homoserinyl-based phosphoramidate acid-cleavable linker. Kinetics of payload release from the scaffold was observed in buffers representing the pH conditions of systemic circulation, early and late endosomes, and lysosomes. It was found that payload release takes place in two key consecutive steps: (1) P−N bond hydrolysis and (2) spacer immolation. These two steps were found to follow pseudo-first-order kinetics and had opposite dependencies on pH. P−N bond hydrolysis increased with decreasing pH, while spacer immolation was most rapid at physiological pH. Despite the contrasting release kinetics of these two steps, maximal payload release was observed at the mildly acidic pH (5.0−5.5), while minimal payload release occurred at physiological pH. We integrated this phosphoramidate-payload linker system into a PSMA-targeted fluorescent turn-on probe to study the intracellular trafficking and release of a fluorescent payload in PSMA-expressing prostate cancer cells. Results showed excellent turn-on and accumulation of the coumarin payload in the late endosomal and lysosomal compartments of these cells. The release properties of this linker mark it as an attractive alternative in the modular design of ADCs and SMDCs, which demand selective intracellular payload release triggered by the pH changes that accompany intracellular trafficking.

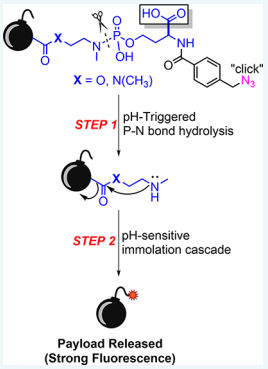

1. INTRODUCTION

It is estimated that 608,570 individuals will die of cancer-related complications in the United States in 2021.[1] The types of treatment received depend exclusively on the type of cancer and how advanced it is. Many cancer patients receive conventional chemotherapy, which interferes with DNA replication or cell division, thus killing proliferating cells, which in theory are cancerous. Unfortunately, many current chemotherapeutic drugs have limited specificity and often result in deleterious effects on healthy peripheral tissues.[2,3] Thus, there is an obvious need for therapies with increased specificity and reduced toxicity.

Over the past two decades, antibody drug conjugates (ADCs)[4−7] and, to a lesser degree, small-molecule drug conjugates[8−10] (SMDCs) have begun to address these issues, with ADCs being the most efficacious. A successful drug conjugate (DC) comprises three design elements. First, the DC must contain a targeting molecule (e.g., antibody or high-affinity ligand) for a cell surface cancer biomarker. Once a DC is successfully bound to a cell surface cancer biomarker, it is internalized through receptor-mediated endocytosis and proceeds through a series of steps that can include (a) hydrolytic degradation under acidic conditions of subcellular organelles; (b) proteolytic degradation by lysosome-abundant proteases; or (c) disulfide cleavage by glutathione. An example of one of these tumor-specific cell surface targets, prostate-specific membrane antigen (PSMA), has been used as a reliable clinical biomarker for the detection and localization of prostate cancer because of its specific upregulation in approximately 80% of tumor epithelial cells during prostate cancer progression, where it correlates negatively with prognosis.[11−14] Inhibitors (phosphoramidates and urea) of PSMA's enzymatic activity have been used as PSMA-targeting molecules for various imaging[15−29] and therapeutic agents.[30−35] Despite considerable efforts to outfit small-molecule PSMA-targeting agents with cytotoxic drugs,[36] a few PSMA-targeted SMDCs have been effective because of insufficient internalization into tumor cells. Regardless, many PSMA-targeted molecules are currently in clinical trials, with piflufolastat F-18[37] and 68Ga-PSMA-11[38,39] recently receiving FDA approval, highlighting the continued interest in PSMA in biomedical, translational medicine, and pharmaceutical fields.[40]

The second element of a successful DC is that it must contain a cytotoxic payload such as the chemotherapeutic agent

Received: September 7, 2021
Revised: October 8, 2021
Published: October 26, 2021

https://doi.org/10.1021/acs.bioconjchem.1c00435
Bioconjugate Chem. 2021, 32, 2386−2396

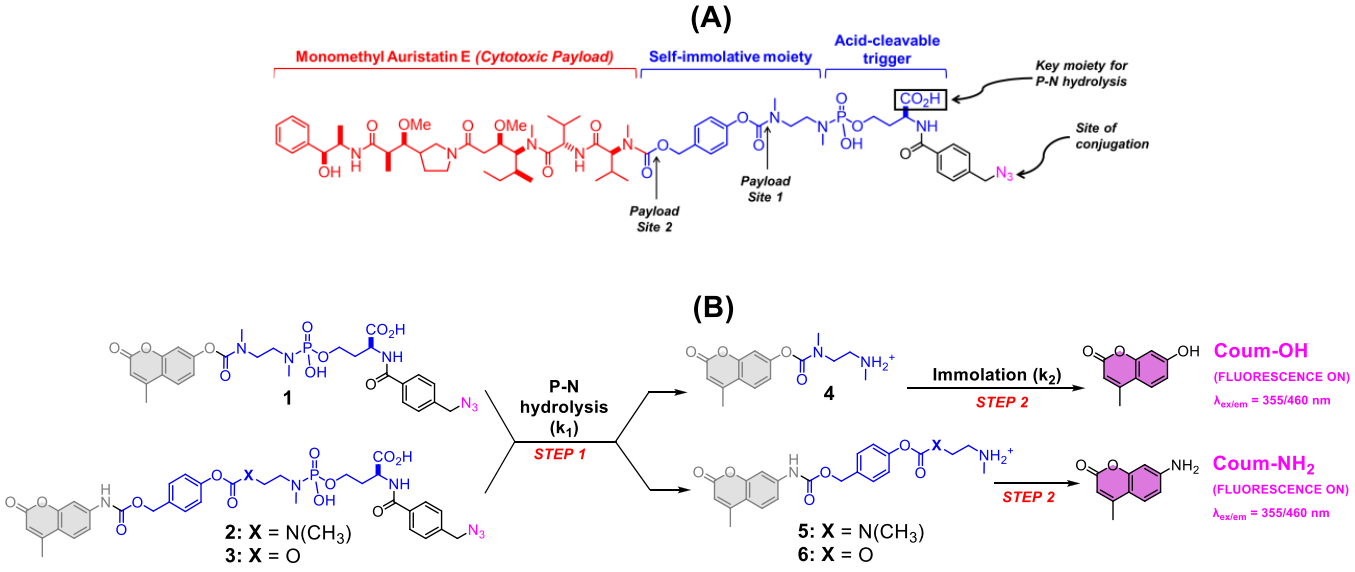

Figure 1. (A) Representation of the acid-cleavable phosphoramidate-payload system from prior studies. (B) Overview of the stepwise release and turn-on of latent fluorophores described in this study. k_1 and k_2 are rate constants for P−N bond hydrolysis and immolation, respectively.

Scheme 1. Synthesis of 1, 2, and 3 Was Achieved via a Two-Step Procedure from Key Alcohol Intermediates[a]

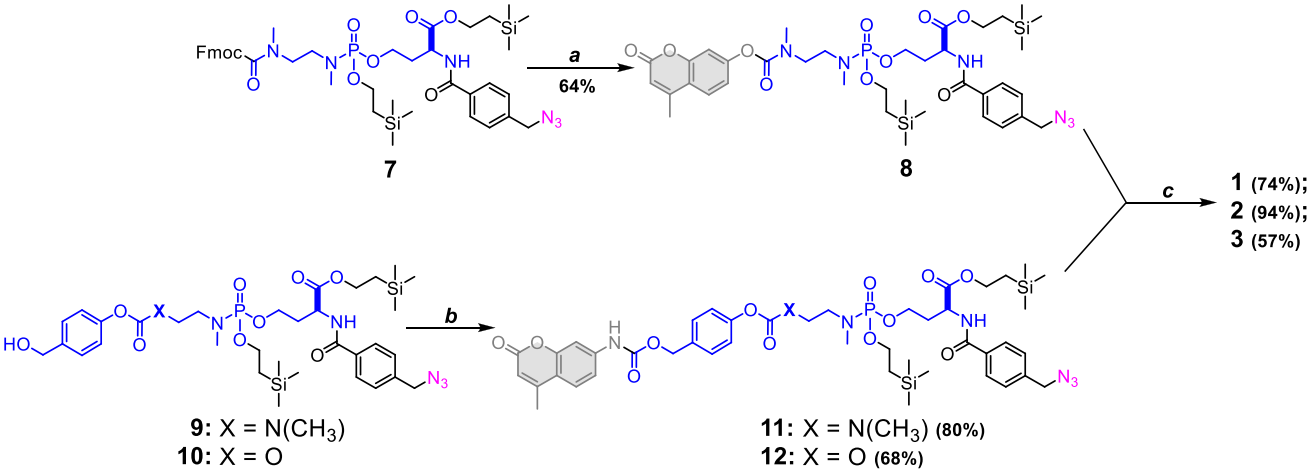

[a]Reaction conditions and yields (a) **Coum-OCOCl**, cat. DBU, DIPEA, CH_2Cl_2 (b) **Coum-NCO**, Et_3N, CH_2Cl_2 (b) CsF, 18-Crown-6, DMF.

monomethyl auristatin E (MMAE). Third, a DC must contain a cleavable linker to couple the payload to the targeting molecule for facile release of the payload in targeted cells. Acid-cleavable linkers are considered to be the most desirable yet the most challenging to incorporate into DC applications. Acid-cleavable linkers are specifically designed to remain stable at the neutral pH of serum and plasma, which is extremely important for efficient and safe drug delivery. However, these linkers can present a challenge in terms of extracellular stability within the low pH hypoxic, tumor microenvironment as they can undergo premature, spontaneous release of the cytotoxic payload and damage normal surrounding tissues as well as target cells through a bystander effect. To date, only two ADCs[41−43] (Mylotarg and Besponsa) utilizing an acid-degradable hydrazone linker have been approved for clinical use.

We have recently reported on the development of an acid-cleavable phosphoramidate-based linker capable of releasing MMAE (Figure 1A).[44] This linker contains two key structural components: (1) a biologically stable and cleavable pH-triggered phosphoramidate scaffold and (2) a self-immolative spacer. MMAE is released when the self-immolative spacer is hydrolyzed from the phosphoramidate scaffold through exposure to acidic conditions. Once hydrolyzed, the self-immolative moiety undergoes ordered degradation, triggering a clean release of MMAE. Additionally, this linker is click-ready and water-soluble to aid bioconjugation to an array of relevant therapeutic targeting agents.

Here, we describe the versatility and potential therapeutic applicability of this phosphoramidate-based linker to effectively release amine- and alcohol-functionalized fluorogenic coumarin payloads at various acidic pH values characteristic of the endosomal and lysosomal compartments[45,46] encountered during receptor-mediated endocytosis. As proof of principle, we used the extracellular, enzymatic domain of the biomarker PSMA as a target to demonstrate the internalization and release of the fluorogenic coumarin payload into immortalized human prostate cancer cells via receptor-mediated endocytosis.

https://doi.org/10.1021/acs.bioconjchem.1c00435
Bioconjugate Chem. 2021, 32, 2386−2396

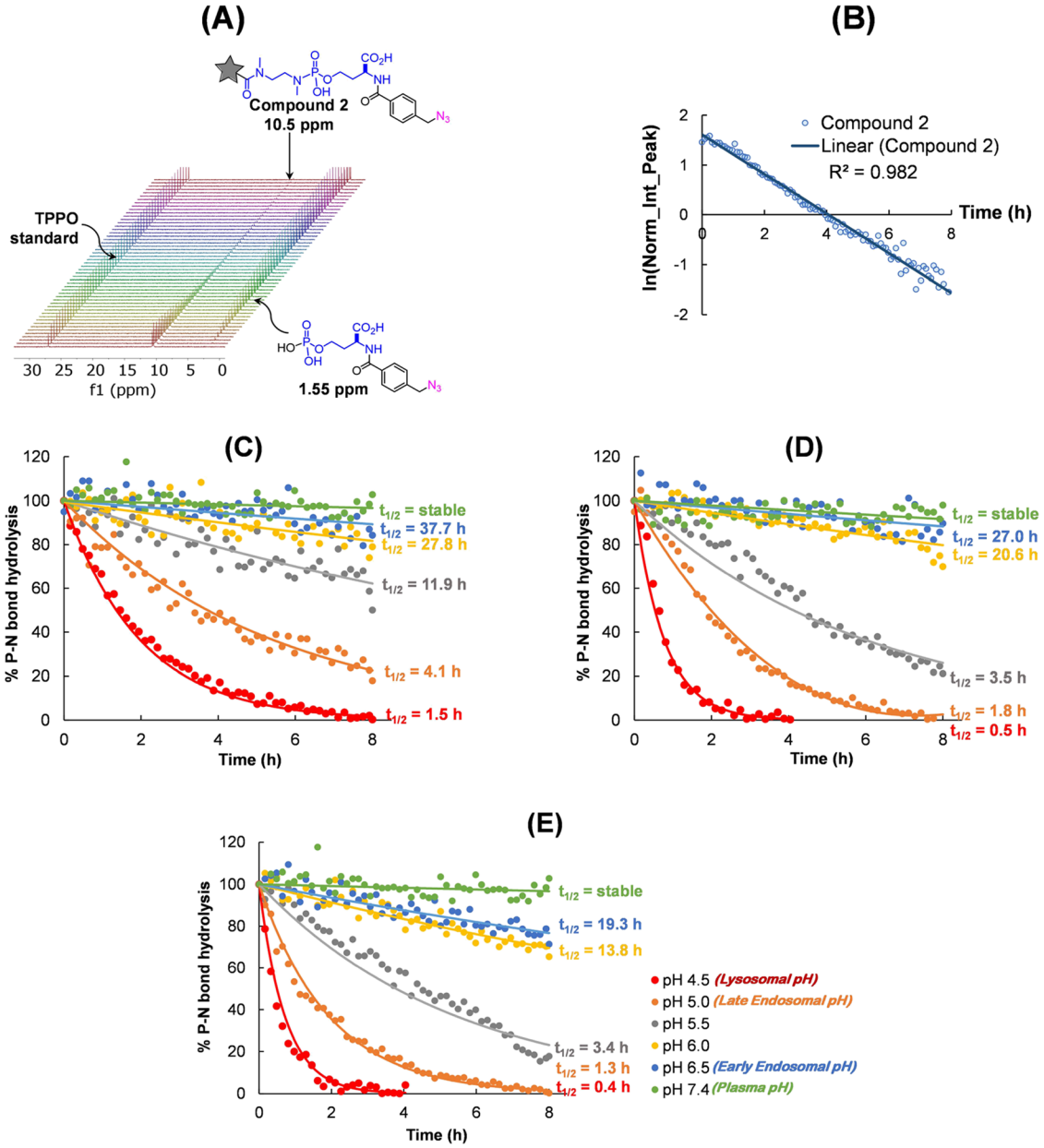

Figure 2. (A) Raw stacked NMR data for **2** (10.5 ppm) at pH 5.0. The peak at 1.55 ppm is the hydrolytic product. (B) Semi-log transformation of the compiled data for the area under the curve of **2** normalized to the standard, illustrating first-order kinetics. Scatter plot and their exponential fit showing %P−N bond hydrolysis (reported as half-lives) vs time at pH 4.5, 5.0, 5.5, 6.0, 6.5, and 7.4 for compound (C) **1**; (D) **2**; and (E) **3**. Each study was carried out for 8 h.

2. RESULTS AND DISCUSSION

2.1. Assembly of the Acid-Labile Turn-on Dye Modules. The acid-labile turn-on dye modules comprised a phosphoramidate moiety coupled to a latent fluorescent payload through one or two self-immolative spacers (Figure 1B). Compound **1** was designed to explore the release of phenol-based payloads (e.g., 4-methylumbelliferone, **Coum-OH**), while compounds **2** and **3** were designed to release aniline-based payloads (e.g., 7-amino-4-methylcoumarin, **Coum-NH$_2$**). Synthesis of **1** was achieved via the reaction of Fmoc-protected intermediate **7** in a DBU-facilitated deprotection, followed by reaction with hymecromone chloroformate all in one-pot to yield silyl-protected phosphoramidate **8**. Global O-silyl deprotection of **8** afforded **1** in good yield (Scheme 1). The preparation of **2** and **3** was achieved via the reaction of alcohols **9** and **10** with 7-amino-4-methylcoumarin isocyanate, followed by global O-silyl deprotection. Of note, the rationale for substituting the carbamate *N*-methyl group in **2** with oxygen in compound **3** was to determine if there would be an advantage to more rapid immolation.[46]

2.2. pH-Dependent Hydrolysis Kinetics of the P−N Bond in the Acid-Labile Turn-on Dye Modules. Once prepared, the hydrolytic P−N bond degradation of turn-on dye modules **1**−**3** was monitored by ^{31}P NMR in buffers ranging from pH values of 4.5 (lysosomal pH), 5.0 (late endosomal pH), 5.5, 6.0, 6.5 (early endosomal pH), and 7.4 (physiological pH) over 8 h at 37 °C. The NMR array data were compiled using MNova 14.1 software, and the peak area for each compound was normalized to a constant concentration of an external standard

https://doi.org/10.1021/acs.bioconjchem.1c00435
Bioconjugate Chem. 2021, 32, 2386−2396

(triphenylphosphine oxide, TPPO), as shown for compound **2** as a representative example in Figure 2A.

As anticipated, the rate of P−N bond hydrolysis of the payload-phosphoramidate system **1**−**3** followed pseudo-first-order kinetics at all pH values (Figure 2B), consistent with our initial studies.[44,47,48] The rate constants (k_1) are summarized in Table 1. Importantly, there was no detectable hydrolysis

Table 1. pH-Dependent Rate Constants for P−N Bond Hydrolysis (k_1) and Spacer Immolation (k_2)

	compound **1**		compound **2**		compound **3**	
pH	k_1 (h^{-1})	k_2 (h^{-1})	k_1 (h^{-1})	k_2 (h^{-1})	k_1 (h^{-1})	k_2 (h^{-1})
4.5	0.46	0.063	1.39	0.011	1.73	0.73
5.0	0.17	0.12	0.39	0.034	0.53	1.35
5.5	0.058	0.32	0.20	0.082	0.20	2.70
6.0	0.025	0.79	0.034	0.097	0.050	7.20
6.5	0.018	2.32	0.026	0.20	0.036	22.5
7.4	stable	12.6	stable	1.56	stable	unstable

observed for the modules at physiological pH (Figure 2C−E). Because the release of the payload is predicated on the initial hydrolysis of the P−N bond, the linker stability at physiological pH is expected to mitigate off-target effects typified by the premature degradation of linker-payload systems in systemic circulation. While the rates of P−N bond hydrolysis for the turn-on dye modules were generally similar across all pH values, a progressive decrease in the hydrolytic half-lives was observed as the pH dropped from 6.5 (early endosomal) to 4.5 (lysosomal). The similarities in half-lives for these three linkers indicate that the nature of the payload does not interfere with the release kinetics at the P−N bond of the phosphoramidates.

2.3. pH-Dependent Kinetics of Fluorophore Release from Self-Immolative Spacers. We prepared the individual spacer-dye modules (**4**−**6**) to study specifically the pH-dependence of the self-immolative release, and concomitant turn-on, of the latent fluorophores that would be independent of P−N hydrolysis. While P−N bond hydrolysis is known to be promoted by acidic conditions,[44,47−50] the opposite was observed to be true for the self-immolation of the *N,N′*-dimethylethylenediamine spacer. To prepare the modules (**4**−**6**) (Scheme 2), Boc-protected amine (**13**) and alcohols (**14, 15**) were reacted with activated fluorogenic payloads (**Coum-OCOCl** and **Coum-NCO**), as depicted in Scheme 2. Boc-deprotection of intermediates **16**−**18** with 4 N HCl in 1,4-dioxane solution provided the desired modules as amine-HCl salts. The time-dependent fluorescent turn-on kinetics of the spacer-dye modules (**4**−**6**) were carried out for 6 h at 37 °C in buffers mimicking physiological and relevant intracellular compartment pH values, with the corresponding time course of fluorescence recorded at λ = 460 nm (excitation at λ = 355 nm).

The rate of immolation for the spacer-dye modules (**4**−**6**) was found to be proportionally dependent on the pH (Figure 3). The rate constants (k_2) are summarized in Table 1. As expected, immolation rates decreased with a decrease in pH as the acid−base equilibrium favors the non-nucleophilic conjugate acid form of the spacer-payload module, as illustrated in Scheme 3 for compound **4** as a representative example. Hence, the nucleophilicity of the *N,N′*-dimethylethylenediamine spacer is diminished and cannot initiate spontaneous cyclization that forms *N,N′*-dimethylimidazolidinone and concomitantly releases the payload. It was also noted that the pH-dependence of the immolation rate was not concentration-dependent (Figure 3A, inset). At concentrations of both 1 and 10 μM for compound **4**, the linear relationship between the immolation rate and pH was similar, suggesting first-order kinetics. This is typical for reactions with an acid−base pre-equilibrium, where only the electron-rich conjugate base undergoes the rate-determining step (Scheme 3).[51]

It is noteworthy that compound **5** exhibited slower release kinetics (Figure 3B) compared to that of **4** (Figure 3A). Unlike compound **4**, the phenol released in compound **5** after the immolation of the *N,N′*-dimethylethylenediamine spacer undergoes an additional 1,6-elimination cascade to release para-quinone methide, CO_2, and the fluorescent payload. It is likely that the slower release kinetics of compound **5** are due to this additional immolative step. Furthermore, this slower release can also be attributed to the *p*-hydroxylmethyl phenol moiety in compound **5** (p*K*a = 9.7) being a poor leaving group compared to the coumarin payload (p*K*a = 7.8) found in compound **4**.

Unlike compounds **4** and **5**, the carbamate *N*-methyl group in the *N,N′*-dimethylethylenediamine spacer was replaced with oxygen in compound **6**. This substitution, providing a more electrophilic carbonate, was expected to allow for more rapid cyclization of the *N*-methylethanolamine spacer to 3-methyloxazolidin-2-one (Figure 3C). Indeed, the payload release from **6** was found to be considerably more rapid at all pH values than that from compounds **4** and **5**.

2.4. pH-Dependent Kinetics of Fluorophore Release from the Acid-Labile Turn-on Dye Modules. The pH-triggered release of the latent fluorogenic payloads from the turn-on dye modules **1**, **2**, and **3** was evaluated in buffers ranging from pH 4.5 to 7.4 at 37 °C over 18 h. The resulting fluorescence

Scheme 2. Synthesis of 4, 5, and 6 Was Achieved via a Two-Step Procedure from Key Alcohol Intermediates[a]

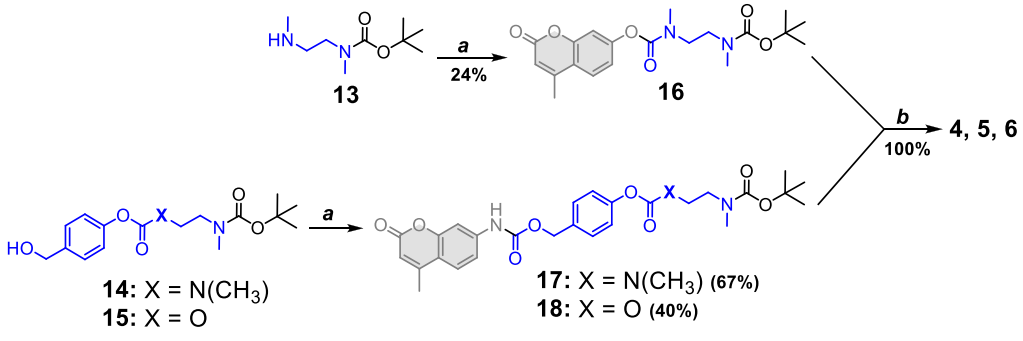

[a]Reaction conditions and yields (a) **Coum-OCOCl** or **Coum-NCO**, Et_3N, CH_2Cl_2 and (b) 4 N HCl-1,4-dioxane.

https://doi.org/10.1021/acs.bioconjchem.1c00435
Bioconjugate Chem. 2021, 32, 2386−2396

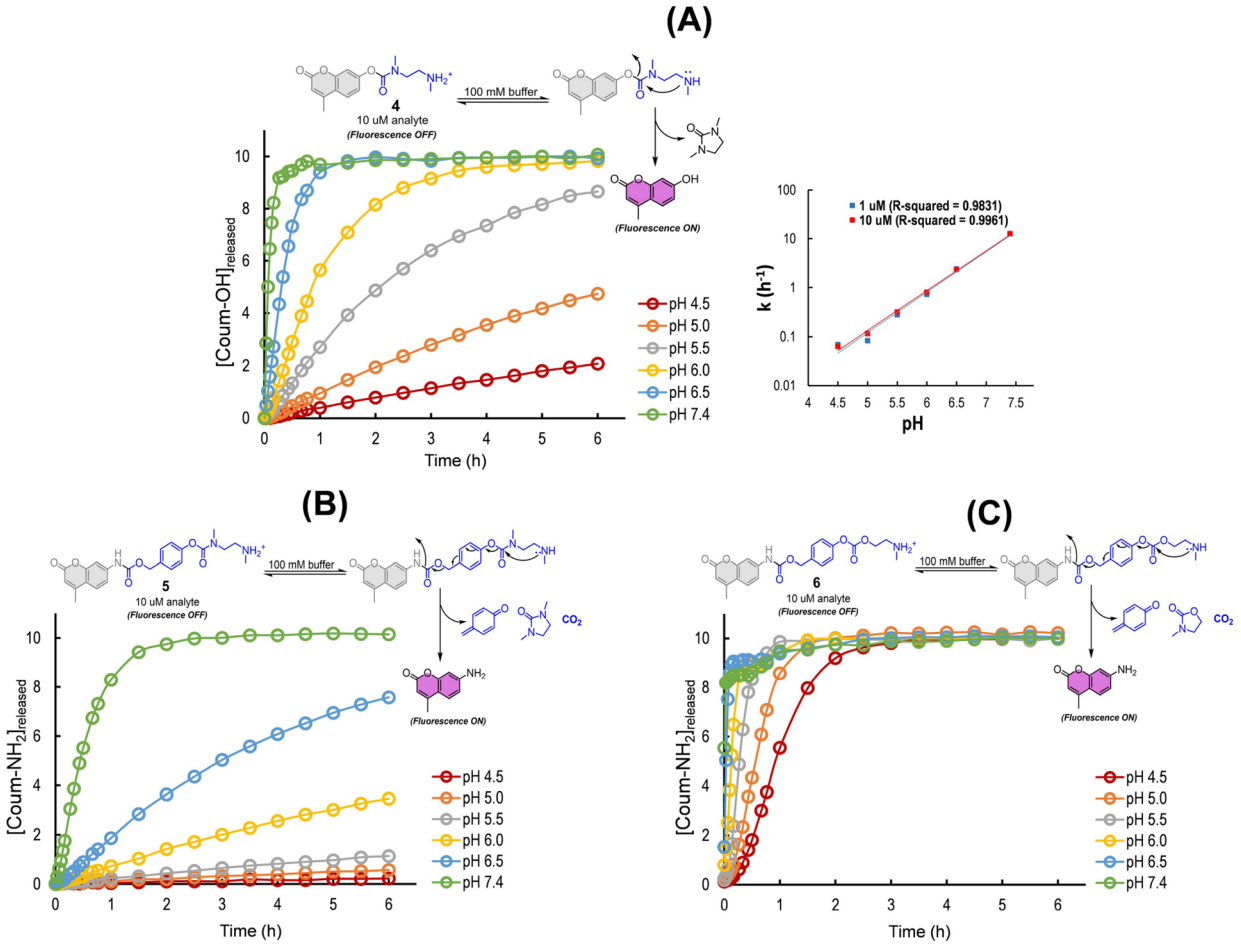

Figure 3. Time-dependent fluorescence studies on the spacer-payload system carried out for 6 h. pH-dependent immolation profiles of (A) Compound **4**, INSET: Semi-log plot of k (h^{-1}) vs pH. (B) Compound **5**. (C) Compound **6**.

Scheme 3. Mechanism of Payload Release from Phosphoramidate-Payload System Highlighting the Two Key Steps: P−N Bond Hydrolysis and Immolation

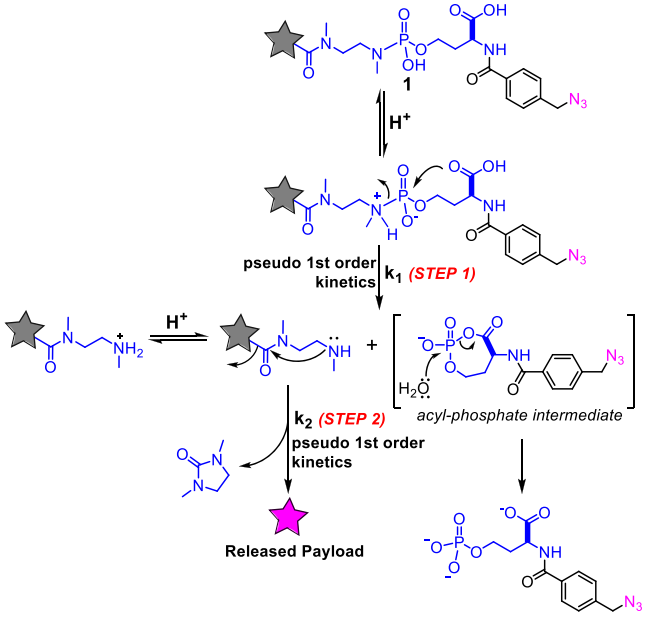

of the released dyes was recorded at λ = 460 nm (excitation at 355 nm). Mechanistically (Scheme 3), the release of the payload from the acid-labile turn-on dye modules is dependent on the two consecutive reactions (P−N bond hydrolysis k_1 and spacer immolation k_2), oppositely dependent upon pH, and the amount of payload released is correlated to the contribution of the two rate constants (k_1 and k_2) associated with these two steps (Table 1). Of note, no payload release was observed for compounds **1** and **2** at physiological pH (Figure 4A,B). This was expected because despite the rapid immolation observed for the spacer units in these compounds at pH 7.4, their P−N bond was stable. Maximal dye release was observed at pH 5.0 for compound **1** and at pH 5.5 and 5.0 for compound **2**. This can be explained by the observation that while at pH 4.5, P−N bond hydrolysis is rapid (k_1), and the rate of spacer immolation to release the dye (k_2) is sluggish.

Compound **3** exhibited a pH-dependent payload-release trend (Figure 4C) reminiscent of its P−N bond hydrolysis rates (Table 1). This is largely due to the spacer immolation rates (k_2) for this compound being generally rapid at all pH values examined, resulting in the P−N bond hydrolysis generally being the rate-limiting step. Surprisingly, we observed dye release at pH 7.4, a condition at which the P−N bond was observed to be stable. We attributed this observation to the hydrolysis of the carbonate moiety, thus triggering the dye release prior to P−N bond hydrolysis. As such, we have concluded that the scaffold of compound **3** would not be suitable in the development of drug conjugates as it would likely lead to premature drug release, leading to off-target effects.

https://doi.org/10.1021/acs.bioconjchem.1c00435
Bioconjugate Chem. 2021, 32, 2386−2396

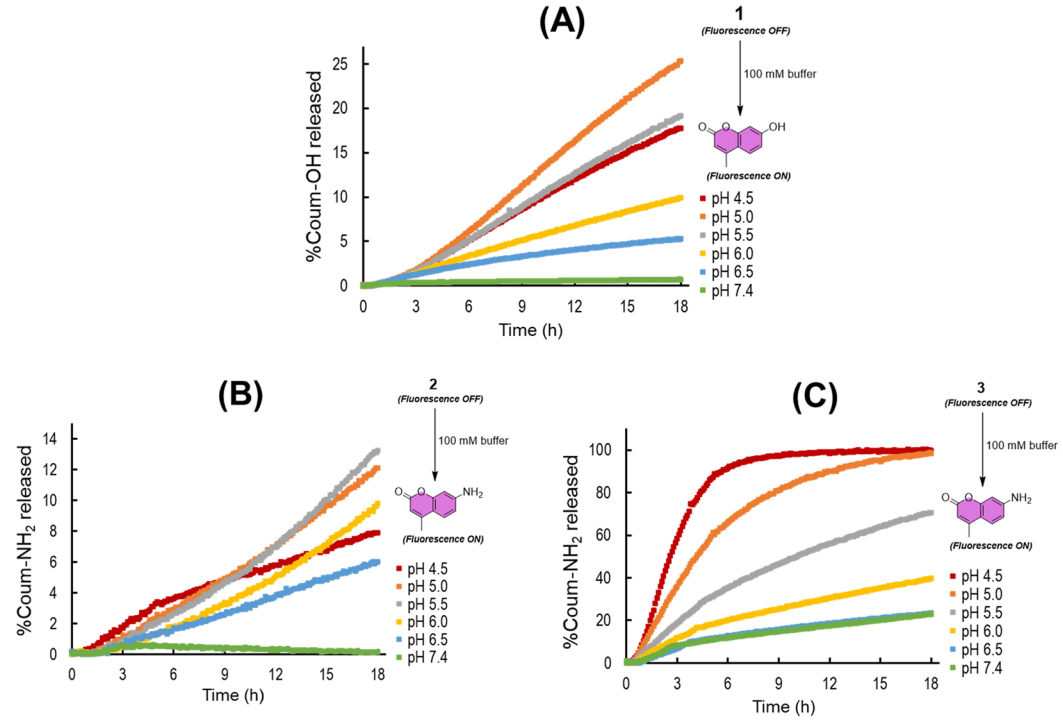

Figure 4. Scatter plots showing the percentage of payload released for (a) Compound **1**, (b) Compound **2**, and (c) Compound **3.**

Scheme 4. Synthesis of PSMA-Targeting Turn-on Probe, Coum-SMDC

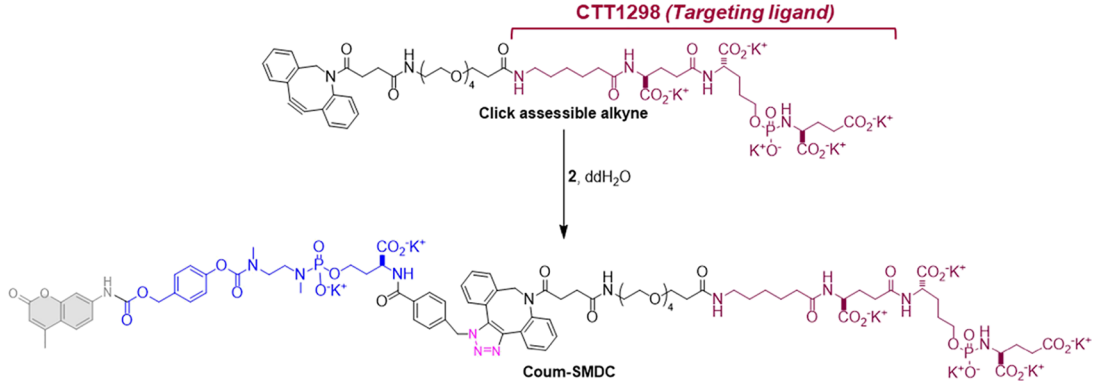

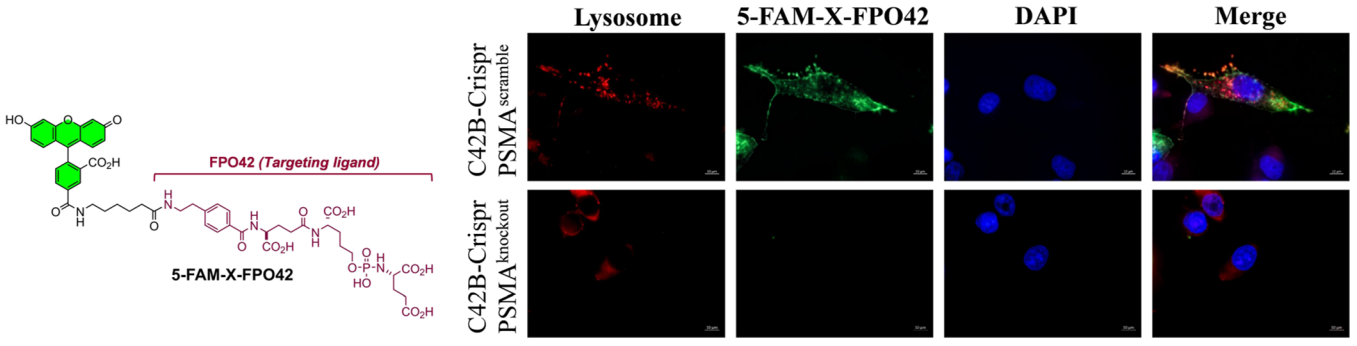

Figure 5. 5-FAM-X-FPO42 binds cell surface PMSA and is internalized via receptor-mediated endocytosis. Immunofluorescent microscopy imaging of C42B-Crispr-PSMA^{scramble} and C42B-Crispr-PSMA^{knockout} cells incubated with **5-FAM-X-FPO-42** and Lysotracker Red DND-99. 63x oil.

2.5. In Vitro Evaluation of a PSMA-Targeted Turn-on Probe. We next investigated the in vitro applicability of the acid-labile turn-on dye modules in the context of a clinically relevant biomarker-targeted probe. Using click chemistry, we coupled the acid-labile turn-on dye module **2** to the PSMA-targeting molecule **CTT1400**[34] to form the PSMA-targeted turn-on probe **Coum-SMDC** (Scheme 4). **CTT1400** is known to irreversibly bind to the enzymatic domain of the tumor-specific cell surface receptor PSMA on prostate tumor cells, which is then followed by rapid and extensive internalization via

https://doi.org/10.1021/acs.bioconjchem.1c00435
Bioconjugate Chem. 2021, 32, 2386−2396

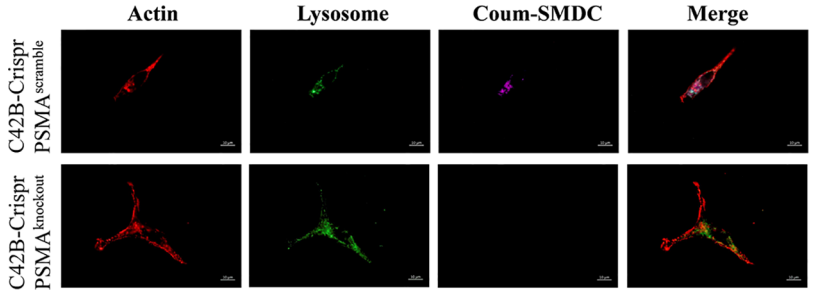

Figure 6. Coum-SMDC releases its payload in the low pH environment of the lysosome. Immunofluorescent microscopy imaging of C42B-Crispr-PSMA^{Scramble} (PSMA+) and C42B-Crispr-PSMA^{knockout} (PSMA−) cells incubated with Actin, Lysotracker Green DND-26, and **Coum-SMDC**. 63x oil.

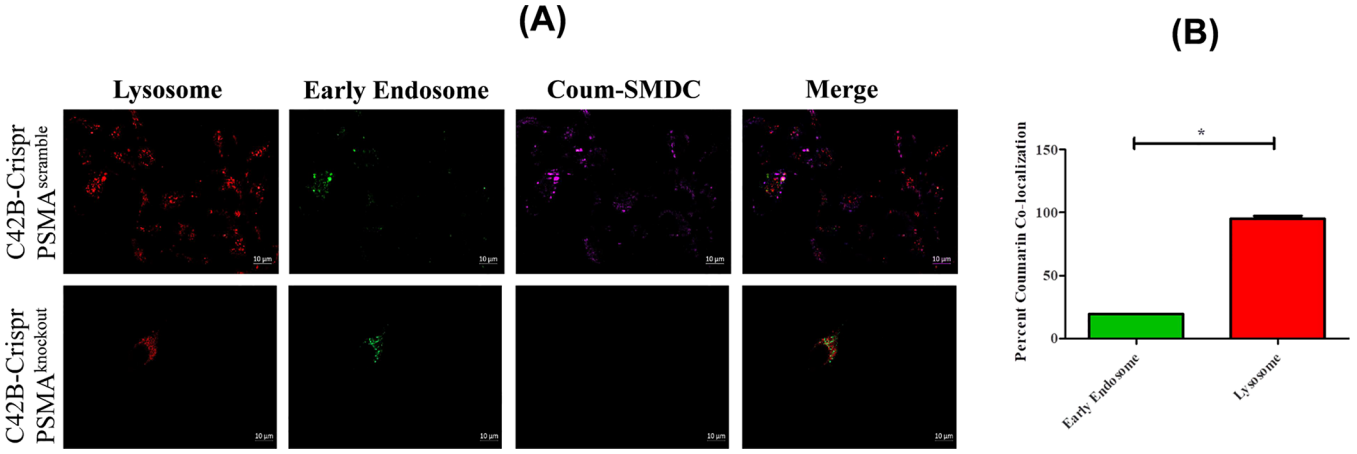

Figure 7. (A) **Coum-SMDC** releases minimal payload first in the early endosome. Immunofluorescent microscopy imaging of C42B-Crispr-PSMA^{scramble} and C42B-Crispr-PSMA^{knockout} cells incubated with Lysotracker Red DND-99, CellLight Early Endosome-GFP tracker, and **Coum-SMDC**. 63x oil. (B) Comparison of percentage coumarin released in early endosome vs lysosome ($n = 3$, $p < 0.05$).

receptor-mediated endocytosis.[34] In addition, we have shown that PSMA is largely tolerant of various pendant groups tethered to phosphoramidate-based small-molecule ligands that target its active site.[52−56] Indeed, the IC_{50} for **Coum-SMDC** against PSMA was 1.4 nM (see Supporting Information Section S6). For proof of in vitro applicability, we created functionally manipulated PSMA CRISPR (clustered regularly interspaced short palindromic repeats) immortalized human prostate cancer C42B cell line (see Supporting Information Section S3) to use as a model. To demonstrate that the PSMA-positive C42B-Crispr-PSMA^{Scramble} and PSMA-negative C42B-Crispr-PSMA^{knockout} cell models were appropriate for this experiment, we first verified that the C42B-Crispr-PSMA^{Scramble} cells expressed cell surface PSMA and that the PSMA could be internalized via receptor-mediated endocytosis. Both C42B-Crispr-PSMA^{scramble} and C42B-Crispr-PSMA^{knockout} were incubated for 30 min with both the PSMA-specific SMDC **5-FAM-X-FPO-42**, which binds exclusively to, and blocks, the enzymatic domain of extracellular, membrane-bound PSMA. Fluorescence microscopy indicated that the C42B-Crispr-PSMA^{Scramble} cells were indeed positive for cell surface PMSA, and 59.81% of the **5-FAM-X-FPO-42**-bound PSMA was internalized into the lysosomes (Figure 5 and Supporting Information Section S3).

In the disease state, epithelial cells located deep within a poorly vascularized tumor, such as those in advanced prostate cancer, can undergo moderate to severe hypoxia and potentially necrosis.[57−60] Lactic acid production and accumulation during these anaerobic conditions results in a local pH drop from 7.4 to 6.7.[59] Therefore, the pH sensitivity and specificity of an SMDC within the therapeutic setting is tremendously important to prevent the untoward consequences of the bystander effect.[61] We previously established that the maximal dye release for compound **2** was pH 5.0 (Figure 4B). Therefore, to assess the ability of **Coum-SMDC** to not only bind successfully to cell surface PSMA but to also release its payload in the low pH environment of the lysosome and the late endosome (pH 4.5−5.5), C42B-Crispr-PSMA^{knockout} and C42B-Crispr-PSMA^{Scramble} cells were treated with **Coum-SMDC** and LysoTracker and incubated for 30 min. Results showed the colocalization of the fluorescent coumarin-derived signal within the lysosomes of the C42B-Crispr-PSMA^{Scramble} but not in the C42B-Crispr-PSMA^{knockout}, signifying that **Coum-SMDC** successfully bound to cell surface PSMA was trafficked to the low pH environment of the lysosome and released its fluorogenic payload (Figure 6).

To further confirm that the PSMA-targeted turn-on probe **Coum-SMDC** was indeed acting in a pH-specific manner in vitro and did not release its payload within the slightly acidic early endosome (pH of 5.9−6.8), which is akin to the disease-generated hypoxic microenvironment, the C42B-Crispr-PSMA^{knockout} and C42B-Crispr-PSMA^{Scramble} cells were incubated with CellLight Early Endosomes-GFP tracker overnight and then treated with **Coum-SMDC** for 30 min (Figure 7A). Results showed that 98.8% of the released fluorescent coumarin dye colocalized with the lysosomes of the C42B-Crispr-PSMA^{Scramble}, while 19.2% colocalized with the early endosomes (Figure 7B). It should be noted that there is a 14.0% overlap in signals, which likely occurs in the endosomes that are transitioning from early to late and theoretically would have a lower pH similar to that of the lysosome. If this is indeed the

https://doi.org/10.1021/acs.bioconjchem.1c00435
Bioconjugate Chem. 2021, 32, 2386−2396

case, only 5.19% of the signal is coming from the early endosome.

3. CONCLUSIONS

The acidic nature of cellular compartments can be co-opted for the triggered release of cell-targeted payloads through acid-cleavable linkers. With respect to cancer therapeutic development, such applications include ADCs and SMDCs, which carry cytotoxic cargo. Herein, we have reported the utility of our acid-cleavable phosphoramidate-based linker scaffolds[47−49] for the pH-triggered release of both amine- and alcohol-functionalized payloads, which in this case were latent fluorogenic coumarin-based dyes. These turn-on probes (compounds **1**−**3**) allowed for the exploration of the key consecutive kinetic steps (P−N bond hydrolysis and spacer immolation) implicated in the eventual degradation of the linker and subsequent release of payloads. While both degradation steps were found to be pH-dependent, the individual rates of the two steps had opposite dependencies on pH. In particular, the rate of spacer immolation was greatest at pH 7.4, while the rate of P−N bond hydrolysis was slowest under this condition, but most rapid at pH 4.5.

In the context of cell-targeted payload-conjugates (such as ADCs and SMDCs), the duality of pH dependence of P−N bond hydrolysis and spacer immolation presents a conundrum in the optimization of intracellular cargo release as the pH drops from 7.4 to 4.5 through the cellular internalization process. That is, P−N bond hydrolysis increases as intracellular pH decreases, while the second step of spacer immolation and payload release begins to decrease. Therefore, the interplay between the pH-dependence of the rates for these steps has a direct implication on the amount of payload released under these various pH conditions. As such, it was observed that the greatest amount of payload release for compounds **1** and **2** was at pH 5.0−5.5 (Figure 4A,B), which, in the context of **Coum-SMDC**, was observed as expected that fluorescence turn-on would occur in the late endosomes and/or lysosomes relatively quickly.

In summary, our recently developed acid-cleavable phosphoramidate-based linker scaffold, outfitted with self-immolative spacers, demonstrates suitable stability under physiological conditions (pH 7.4), while effectively releasing cargo under the pH conditions relevant to the internalization of biomarker-targeted conjugates, that being of either lysosomes or late endosomes transitioning to lysosomes. The modularity of their assembly, amenability for click chemistry, and in vitro performance presented in this report mark this pH-triggered scaffold as an attractive platform for the development of biomarker-targeted conjugates such as ADCs and SMDCs. Indeed, the application of this pH-triggered phosphoramidate-based linker scaffold is currently being pursued in our laboratory for the development of analogous PSMA-targeted SMDCs bearing various chemotherapeutic payloads.

4. MATERIALS AND METHODS

4.1. Chemical Synthesis. All synthetic compounds and intermediates, synthetic schemes, procedures, and corresponding spectra are presented in the Supporting Information.

4.2. Kinetics Studies (^{31}P NMR). Following the previously described methods from our laboratory,[44,47−50] with minor modifications, samples were prepared using approximately 15 mg of each compound dissolved in 150 μL of high-performance liquid chromatography (HPLC)-grade MeOH and then mixed with 400 μL of an appropriate buffer. Buffers were chosen based on specific pH values: 4-(2-hydroxyethyl)-1-piperazineethanesulfonic acid (HEPES, 1 M pH 7.4), 2-(*N*-morpholino)-ethanesulfonic acid (MES, 0.5 M pH 6.5), and citric acid (1 M pH 6.0, 5.5, 5.0, and 4.5). Each buffer was prepared and adjusted to ±0.02 pH with 4 M NaOH or 4 M HCl on an AB15 Accumet basic pH meter equipped with an accuTupH Ag/AgCl pH probe (Fisher Scientific, Sommerville, NJ). Stability studies were performed using ^{31}P NMR on a Varian 500 MHz instrument (Agilent Technologies, Santa Clara, CA). The instrument was equilibrated to 37 °C with an acquisition of 64 scans, a relaxation delay of 1 s, an observed pulse of 3.41 μs at 45°, and a preacquisition delay of 185 s. The instrument was locked to an internal standard, triphenylphosphine oxide (TPPO, 40 mM in DMSO-d6), in an axial capillary positioned within the sample solution. Stability data were collected for 8 h or until complete decay was observed. After data acquisition was complete, all ^{31}P chemical shifts were referenced to the internal standard (TPPO, 27 ppm), and the phase was adjusted accordingly. Nuclear magnetic resonance (NMR) experiment files were loaded into the software MestReNova v14.1.2. Phase correction and baseline fitting were performed in the NMR software. Regions corresponding to the control, the starting material, and the product peak were then exported into the software OriginPro 2020 (OriginLab Corporation, Northampton, MA 01060 USA). The intensities of each peak were normalized to the intensity of the internal triphenylphosphine oxide standard. A first-order decaying linear fitting function was applied to a plot of ln(normalized intensity) of the decaying parent compound versus time. The half-life ($t_{1/2}$) of each compound at the designated pH was then calculated as shown below:

$$t_{1/2} = \frac{\ln 2}{|\text{slope}|}$$

4.3. Kinetic Studies (Fluorescence Spectroscopy). A Fluostar Omega Microplate reader running Omega software version 1.02 and Mars Data Analysis Software Program version 1.10 (BMG Labtech) were used to conduct the time-dependent kinetics studies. Studies were performed in Greiner Bio-One μClear Bottom 96-well 96 plates at 37 °C using hymecromone and 7-amino-4-methylcoumarin as the fluorogenic reporters, monitoring at λ_{ex} = 355 nm and λ_{em} = 460 nm. Assays were performed in the following 100 mM buffers: HEPES (pH 7.4), MES (pH 6.5), and citric acid (pH 6.0, 5.5, 5.0, and 4.5). Stock solutions (10 mM) of each compound (**1**−**6**) were prepared in ddH_2O, and 10 mM stock solutions of fluorogenic reporters (**Coum-OH** and **Coum-NH$_2$**) were prepared in EtOH. All solutions were serially diluted to 100 μM working solutions with ddH_2O. Calibration curves were carried out on the fluorogenic reporters at concentrations of 1 nM−100 μM at each pH value, with the linear range found to be between 10 nM−10 μM. Reactions were initiated by the addition of 20 μL of probe (100 μM working solution) to wells containing 180 μL of buffer, with the total well volume of 200 μL. Product formation was followed for 6 h, with time points recorded at 2 min intervals or for 18 h with time points recorded at 6 min intervals. The fluorescence values in each reaction well were normalized to the maximal fluorescence value in the control well (10 μM of fluorogenic reporters). Rate constants were extracted from GraphPad Prism 9.0 by fitting the data to one phase association model.

4.4. PSMA IC$_{50}$ for Coum-SMDC. The routine determination of IC$_{50}$ for Coum-SMDC was performed, as most

https://doi.org/10.1021/acs.bioconjchem.1c00435
Bioconjugate Chem. 2021, 32, 2386−2396

recently described in our laboratory,[62] using concentrations of 100, 30, 10, 3, and 1 nM.

4.5. Cell Imaging Studies. Cells were plated onto coverslips at a concentration of 1×10^5 cells/well in 1 mL of growth medium and allowed to attach overnight. Cells were then starved for 2 h in fetal bovine serum (FBS)-free RPMI and then incubated for 30 min with one or more of the following: 50 nM Lysotracker Red DND-99 (Thermo Fisher, Pittsburgh, PA), 50 nM Lysotracker Green DND-26 (Thermo Fisher, Pittsburgh, PA), and 1 μM 5-FAM-X-FPO-42 or 1 μM Coum-SMDC at 37 °C. To visualize early endosomes, cells were incubated for 16 h with CellLight Early Endosomes-GFP tracker according to manufacturer's instructions (Thermo Fisher, Pittsburgh, PA). For imaging, coverslips were set on ice, rinsed twice in ice-cold phosphate buffered saline (PBS), fixed in ice-cold 10% neutral buffered formalin solution for 15 min, and mounted using diamond mounting media with or without DAPI (Thermo Fisher, Pittsburgh, PA). Zeiss Zen software was used to acquire and process immunofluorescent images. Fiji Image J was used to quantify the mean gray value of the early endosome, lysosome, and coumarin release. All experiments in this study were repeated for a minimum of three independent experiments. Results are presented as mean ± standard error of the mean (SEM). Statistical analysis was performed using the paired, two-tailed t-test. Differences were considered significant at $P < 0{\cdot}05$.

■ ASSOCIATED CONTENT

Supporting Information

The Supporting Information is available free of charge at https://pubs.acs.org/doi/10.1021/acs.bioconjchem.1c00435.

All synthetic compounds and intermediates, synthetic schemes, procedures, and corresponding spectra, as well as validation results for the cell lines used in this study (PDF)

■ AUTHOR INFORMATION

Corresponding Authors

Leslie A. Caromile − *UCONN Health-Center for Vascular Biology, Farmington, Connecticut 06030-3501, United States*; Email: caromile@uchc.edu

Clifford E. Berkman − *Department of Chemistry, Washington State University, Pullman, Washington 99164-4630, United States*; orcid.org/0000-0003-2544-5252; Email: cberkman@wsu.edu

Authors

Feyisola P. Olatunji − *Department of Chemistry, Washington State University, Pullman, Washington 99164-4630, United States*; orcid.org/0000-0002-6429-7072

Emily A. Savoy − *Department of Chemistry, Washington State University, Pullman, Washington 99164-4630, United States*

Mylan Panteah − *UCONN Health-Center for Vascular Biology, Farmington, Connecticut 06030-3501, United States*

Nooshin Mesbahi − *Department of Chemistry, Washington State University, Pullman, Washington 99164-4630, United States*

Armina Abbasi − *Department of Chemistry, Washington State University, Pullman, Washington 99164-4630, United States*

Cresencia M. Talley − *Department of Chemistry, Washington State University, Pullman, Washington 99164-4630, United States*

Christine L. Lovingier − *Department of Chemistry, Washington State University, Pullman, Washington 99164-4630, United States*

Complete contact information is available at: https://pubs.acs.org/10.1021/acs.bioconjchem.1c00435

Notes

The authors declare no competing financial interest.

■ ACKNOWLEDGMENTS

This work and F.P.O. were supported by the National Institutes of Health (R21CA256382 and T32GM8336, respectively). The authors extend their gratitude for technical assistance to Dr. William Hiscox (WSU Center for NMR Spectroscopy), Dr. Gerhard Munske (WSU Laboratory of Biotechnology and Bioanalysis), and Dr. Deobald Lee (Mass Spectrometry Core Laboratory at University of Idaho). In fond memory, C.E.B. dedicates this work to James R. Keeffe, a generous mentor and friend.

■ REFERENCES

(1) Siegel, R. L.; Miller, K. D.; Fuchs, H. E.; Jemal, A. Cancer Statistics, 2021. *CA Cancer J. Clin.* **2021**, *71*, 7−33.

(2) Pal, S. K.; Twardowski, P.; Sartor, O. Critical appraisal of cabazitaxel in the management of advanced prostate cancer. *Clin. Interv. Aging* **2010**, *5*, 395−402.

(3) Cereda, V.; Formica, V.; Massimiani, G.; Tosetto, L.; Roselli, M. Targeting metastatic castration-resistant prostate cancer: mechanisms of progression and novel early therapeutic approaches. *Expert Opin. Investig. Drugs* **2014**, *23*, 469−487.

(4) Khongorzul, P.; Ling, C. J.; Khan, F. U.; Ihsan, A. U.; Zhang, J. Antibody-Drug Conjugates: A Comprehensive Review. *Mol. Cancer Res.* **2020**, *18*, 3−19.

(5) Joubert, N.; Beck, A.; Dumontet, C.; Denevault-Sabourin, C. Antibody−Drug Conjugates: The Last Decade. *Pharmaceuticals* **2020**, *13*, No. 245.

(6) Gauzy-Lazo, L.; Sassoon, I.; Brun, M.-P. Advances in Antibody−Drug Conjugate Design: Current Clinical Landscape and Future Innovations. *SLAS DISCOVERY: Adv. Sci.Drug Discov.* **2020**, *25*, 843−868.

(7) Drago, J. Z.; Modi, S.; Chandarlapaty, S. Unlocking the potential of antibody−drug conjugates for cancer therapy. *Nat. Rev. Clin. Oncol.* **2021**, *18*, 327−344.

(8) Zhuang, C.; Guan, X.; Ma, H.; Cong, H.; Zhang, W.; Miao, Z. Small molecule-drug conjugates: A novel strategy for cancer-targeted treatment. *Eur. J. Med. Chem.* **2019**, *163*, 883−895.

(9) Deonarain, M. P.; Yahioglu, G.; Stamati, I.; Pomowski, A.; Clarke, J.; Edwards, B. M.; Diez-Posada, S.; Stewart, A. C. Small-Format Drug Conjugates: A Viable Alternative to ADCs for Solid Tumours? *Antibodies* **2018**, *7*, No. 16.

(10) Srinivasarao, M.; Galliford, C. V.; Low, P. S. Principles in the design of ligand-targeted cancer therapeutics and imaging agents. *Nat. Rev. Drug Discov.* **2015**, *14*, 203−219.

(11) Heston, W. D. Characterization and glutamyl preferring carboxypeptidase function of prostate specific membrane antigen: a novel folate hydrolase. *Urology* **1997**, *49*, 104−112.

(12) Israeli, R. S.; Powell, C. T.; Fair, W. R.; Heston, W. D. Molecular cloning of a complementary DNA encoding a prostate-specific membrane antigen. *Cancer Res.* **1993**, *53*, 227−230.

(13) Pinto, J. T.; Suffoletto, B. P.; Berzin, T. M.; Qiao, C. H.; Lin, S.; Tong, W. P.; May, F.; Mukherjee, B.; Heston, W. D. Prostate-specific membrane antigen: a novel folate hydrolase in human prostatic carcinoma cells. *Clinic. cancer res.: offic. J. Amer. Ass.Cancer Res* **1996**, *2*, 1445−1451.

(14) Murphy, G. P.; Elgamal, A. A.; Su, S. L.; Bostwick, D. G.; Holmes, E. H. Current evaluation of the tissue localization and diagnostic utility of prostate specific membrane antigen. *Cancer* **1998**, *83*, 2259−2269.
(15) Rosenthal, S. A.; Haseman, M. K.; Polascik, T. J. Utility of capromab pendetide (ProstaScint) imaging in the management of prostate cancer. *Tech. Urol.* **2001**, *7*, 27−37.
(16) Bander, N. H.; Milowsky, M. I.; Nanus, D. M.; Kostakoglu, L.; Vallabhajosula, S.; Goldsmith, S. J. Phase I trial of 177lutetium-labeled J591, a monoclonal antibody to prostate-specific membrane antigen, in patients with androgen-independent prostate cancer. *J. Clin. Oncol.* **2005**, *23*, 4591−4601.
(17) Chu, T. C.; Shieh, F.; Lavery, L. A.; Levy, M.; Richards-Kortum, R.; Korgel, B. A.; Ellington, A. D. Labeling tumor cells with fluorescent nanocrystal-aptamer bioconjugates. *Biosens. Bioelectron.* **2006**, *21*, 1859−1866.
(18) Farokhzad, O. C.; Khademhosseini, A.; Jon, S.; Hermmann, A.; Cheng, J.; Chin, C.; Kiselyuk, A.; Teply, B.; Eng, G.; Langer, R. Microfluidic system for studying the interaction of nanoparticles and microparticles with cells. *Anal. Chem.* **2005**, *77*, 5453−5459.
(19) Foss, C. A.; Mease, R. C.; Fan, H.; Wang, Y.; Ravert, H. T.; Dannals, R. F.; Olszewski, R. T.; Heston, W. D.; Kozikowski, A. P.; Pomper, M. G. Radiolabeled small-molecule ligands for prostate-specific membrane antigen: in vivo imaging in experimental models of prostate cancer. *Clinic. cancer res.: offic. J. Amer. Ass.Cancer Res* **2005**, *11*, 4022−4028.
(20) Gao, X.; Cui, Y.; Levenson, R. M.; Chung, L. W.; Nie, S. In vivo cancer targeting and imaging with semiconductor quantum dots. *Nat. Biotechnol.* **2004**, *22*, 969−976.
(21) Guilarte, T. R.; McGlothan, J. L.; Foss, C. A.; Zhou, J.; Heston, W. D.; Kozikowski, A. P.; Pomper, M. G.; Department of Environmental Health Sciences, U. S. A. Glutamate carboxypeptidase II levels in rodent brain using [125I]DCIT quantitative autoradiography. *Neurosci. Lett.* **2005**, *387*, 141−144.
(22) Humblet, V.; Lapidus, R.; Williams, L. R.; Tsukamoto, T.; Rojas, C.; Majer, P.; Hin, B.; Ohnishi, S.; De Grand, A. M.; Zaheer, A.; Renze, J. T.; Nakayama, A.; Slusher, B. S.; Frangioni, J. V. High-affinity near-infrared fluorescent small-molecule contrast agents for in vivo imaging of prostate-specific membrane antigen. *Mol. Imaging* **2005**, *4*, 448−462.
(23) Milowsky, M. I.; Nanus, D. M.; Kostakoglu, L.; Sheehan, C. E.; Vallabhajosula, S.; Goldsmith, S. J.; Ross, J. S.; Bander, N. H. Vascular targeted therapy with anti-prostate-specific membrane antigen monoclonal antibody J591 in advanced solid tumors. *J. Clin. Oncol.* **2007**, *25*, 540−547.
(24) Pomper, M. G.; Musachio, J. L.; Zhang, J.; Scheffel, U.; Zhou, Y.; Hilton, J.; Maini, A.; Dannals, R. F.; Wong, D. F.; Kozikowski, A. P. 11C-MCG: synthesis, uptake selectivity, and primate PET of a probe for glutamate carboxypeptidase II (NAALADase). *Mol. Imaging* **2002**, *1*, 96−101.
(25) Smith, M. R.; Nelson, J. B. Future therapies in hormone-refractory prostate cancer. *Urology* **2005**, *65*, 9−16 discussion 17.
(26) Smith-Jones, P. M.; Vallabhajosula, S.; Navarro, V.; Bastidas, D.; Goldsmith, S. J.; Bander, N. H. Radiolabeled monoclonal antibodies specific to the extracellular domain of prostate-specific membrane antigen: preclinical studies in nude mice bearing LNCaP human prostate tumor. *J. Nuclear Med.* **2003**, *44*, 610−617.
(27) Tsukamoto, T.; Wozniak, K. M.; Slusher, B. S. Progress in the discovery and development of glutamate carboxypeptidase II inhibitors. *Drug Discov. Today* **2007**, *12*, 767−776.
(28) Ganguly, T.; Dannoon, S.; Hopkins, M. R.; Murphy, S.; Cahaya, H.; Blecha, J. E.; Jivan, S.; Drake, C. R.; Barinka, C.; Jones, E. F.; VanBrocklin, H. F.; Berkman, C. E. A high-affinity [(18)F]-labeled phosphoramidate peptidomimetic PSMA-targeted inhibitor for PET imaging of prostate cancer. *Nucl. Med. Biol.* **2015**, *42*, 780−787.
(29) Dannoon, S.; Ganguly, T.; Cahaya, H.; Geruntho, J. J.; Galliher, M. S.; Beyer, S. K.; Choy, C. J.; Hopkins, M. R.; Regan, M.; Blecha, J. E.; Skultetyova, L.; Drake, C. R.; Jivan, S.; Barinka, C.; Jones, E. F.; Berkman, C. E.; VanBrocklin, H. F. Structure-Activity Relationship of (18)F-Labeled Phosphoramidate Peptidomimetic Prostate-Specific Membrane Antigen (PSMA)-Targeted Inhibitor Analogues for PET Imaging of Prostate Cancer. *J. Med. Chem.* **2016**, *59*, 5684−5694.
(30) Tasch, J.; Gong, M.; Sadelain, M.; Heston, W. D. A unique folate hydrolase, prostate-specific membrane antigen (PSMA): a target for immunotherapy? *Crit. Rev. Immunol.* **2001**, *21*, 13.
(31) Salit, R. B.; Kast, W. M.; Velders, M. P. Ins and outs of clinical trials with peptide-based vaccines. *Front Biosci.* **2002**, *7*, e204−e213.
(32) Lu, J.; Celis, E. Recognition of prostate tumor cells by cytotoxic T lymphocytes specific for prostate-specific membrane antigen. *Cancer Res.* **2002**, *62*, 5807−5812.
(33) Fracasso, G.; Bellisola, G.; Cingarlini, S.; Castelletti, D.; Prayer-Galetti, T.; Pagano, F.; Tridente, G.; Colombatti, M. Anti-tumor effects of toxins targeted to the prostate specific membrane antigen. *Prostate* **2002**, *53*, 9−23.
(34) Choy, C. J.; Ling, X.; Geruntho, J. J.; Beyer, S. K.; Latoche, J. D.; Langton-Webster, B.; Anderson, C. J.; Berkman, C. E. 177Lu-Labeled Phosphoramidate-Based PSMA Inhibitors: The Effect of an Albumin Binder on Biodistribution and Therapeutic Efficacy in Prostate Tumor-Bearing Mice. *Theranostics* **2017**, *7*, 1928−1939.
(35) Ling, X.; Latoche, J. D.; Choy, C. J.; Kurland, B. F.; Laymon, C. M.; Wu, Y.; Salamacha, N.; Shen, D.; Geruntho, J. J.; Rigatti, L. H.; Windish, H. P.; Langton-Webster, B.; Berkman, C. E.; Anderson, C. J. Preclinical Dosimetry, Imaging, and Targeted Radionuclide Therapy Studies of Lu-177-Labeled Albumin-Binding, PSMA-Targeted CTT1403. *Mol. Imaging Biol.* **2020**, *22*, 274.
(36) Wang, X.; Shirke, A.; Walker, E.; Sun, R.; Ramamurthy, G.; Wang, J.; Shan, L.; Mangadlao, J.; Dong, Z.; Li, J.; Wang, Z.; Schluchter, M.; Luo, D.; Wang, Y.; Stauffer, S.; Brady-Kalnay, S.; Hoimes, C.; Lee, Z.; Basilion, J. P. Small Molecule-Based Prodrug Targeting Prostate Specific Membrane Antigen for the Treatment of Prostate Cancer. *Cancers* **2021**, *13*, No. 417.
(37) Keam, S. J. Piflufolastat F 18: Diagnostic First Approval. *Mol. Diagn. Ther.* **2021**, 647.
(38) Fendler, W. P.; Calais, J.; Eiber, M.; Flavell, R. R.; Mishoe, A.; Feng, F. Y.; Nguyen, H. G.; Reiter, R. E.; Rettig, M. B.; Okamoto, S.; Emmett, L.; Zacho, H. D.; Ilhan, H.; Wetter, A.; Rischpler, C.; Schoder, H.; Burger, I. A.; Gartmann, J.; Smith, R.; Small, E. J.; Slavik, R.; Carroll, P. R.; Herrmann, K.; Czernin, J.; Hope, T. A. Assessment of 68Ga-PSMA-11 PET Accuracy in Localizing Recurrent Prostate Cancer: A Prospective Single-Arm Clinical Trial. *JAMA Oncol.* **2019**, *5*, 856−863.
(39) Hadaschik, B.; Ost, P. Re: Assessment of (68)Ga-PSMA-11 PET Accuracy in Localizing Recurrent Prostate Cancer: A Prospective Single-Arm Clinical Trial. *Eur. Urol.* **2019**, *76*, 538−539.
(40) Dassie, J. P.; Hernandez, L. I.; Thomas, G. S.; Long, M. E.; Rockey, W. M.; Howell, C. A.; Chen, Y.; Hernandez, F. J.; Liu, X. Y.; Wilson, M. E.; Allen, L. A.; Vaena, D. A.; Meyerholz, D. K.; Giangrande, P. H. Targeted inhibition of prostate cancer metastases with an RNA aptamer to prostate-specific membrane antigen. *Mol. Ther.* **2014**, *22*, 1910−1922.
(41) Lamb, Y. N. Inotuzumab Ozogamicin: First Global Approval. *Drugs* **2017**, *77*, 1603−1610.
(42) Norsworthy, K. J.; Ko, C. W.; Lee, J. E.; Liu, J.; John, C. S.; Przepiorka, D.; Farrell, A. T.; Pazdur, R. FDA Approval Summary: Mylotarg for Treatment of Patients with Relapsed or Refractory CD33-Positive Acute Myeloid Leukemia. *Oncologist* **2018**, *23*, 1103−1108.
(43) Abe, Y., Sugihara, K., Nakada, T., Shahidi, J., Gallant, G. J. A., Jikoh, T., Agatsuma, T. (2019) ADCs on the Market and in Clinical Development, in *Cancer Drug Delivery Systems Based on the Tumor Microenvironment* (Matsumura, Y., Tarin, D., Eds.) pp. 155−174, Springer Japan, Tokyo, DOI: 10.1007/978-4-431-56880-3_7.
(44) Olatunji, F. P.; Herman, J. W.; Kesic, B. N.; Olabode, D.; Berkman, C. E. A click-ready pH-triggered phosphoramidate-based linker for controlled release of monomethyl auristatin E. *Tetrahedron Lett.* **2020**, *61*, No. 152398.
(45) Scott, C. C.; Gruenberg, J. Ion flux and the function of endosomes and lysosomes: pH is just the start. *Bioessays* **2011**, *33*, 103−110.

https://doi.org/10.1021/acs.bioconjchem.1c00435
Bioconjugate Chem. 2021, 32, 2386−2396

(46) Chen, E. K. Y.; McBride, R. A.; Gillies, E. R. Self-Immolative Polymers Containing Rapidly Cyclizing Spacers: Toward Rapid Depolymerization Rates. *Macromolecules* **2012**, *45*, 7364−7374.
(47) Choy, C. J.; Ley, C. R.; Davis, A. L.; Backer, B. S.; Geruntho, J. J.; Clowers, B. H.; Berkman, C. E. Second-Generation Tunable pH-Sensitive Phosphoramidate-Based Linkers for Controlled Release. *Bioconjug. Chem.* **2016**, *27*, 2206−2213.
(48) Backer, B. S.; Choy, C. J.; Davis, A. L.; Browne, Z. S.; Berkman, C. E. Tunable pH-Sensitive 2-Carboxybenzyl Phosphoramidate Cleavable Linkers. *Tetrahedron Lett.* **2020**, *61*, No. 151650.
(49) Choy, C. J.; Geruntho, J. J.; Davis, A. L.; Berkman, C. E. Tunable pH-Sensitive Linker for Controlled Release. *Bioconjug. Chem.* **2016**, *27*, 824−830.
(50) Olatunji, F. P.; Kesic, B. N.; Choy, C. J.; Berkman, C. E. Phosphoramidate derivates as controlled-release prodrugs of l-Dopa. *Bioorg. Med. Chem. Lett.* **2019**, *29*, 2571−2574.
(51) Müller, I. A.; Kratz, F.; Jung, M.; Warnecke, A. Schiff bases derived from p-aminobenzyl alcohol as trigger groups for pH-dependent prodrug activation. *Tetrahedron Lett.* **2010**, *51*, 4371−4374.
(52) Liu, T.; Toriyabe, Y.; Kazak, M.; Berkman, C. E. Pseudoirreversible Inhibition of Prostate-Specific Membrane Antigen by Phosphoramidate Peptidomimetics. *Biochemistry* **2008**, *47*, 12658−12660.
(53) Liu, T.; Wu, L. Y.; Hopkins, M. R.; Choi, J. K.; Berkman, C. E. A targeted low molecular weight near-infrared fluorescent probe for prostate cancer. *Bioorg. Med. Chem. Lett.* **2010**, *20*, 7124−7126.
(54) Liu, T.; Wu, L. Y.; Kazak, M.; Berkman, C. E. Cell-Surface labeling and internalization by a fluorescent inhibitor of prostate-specific membrane antigen. *Prostate* **2008**, *68*, 955−964.
(55) Nedrow-Byers, J. R.; Jabbes, M.; Jewett, C.; Ganguly, T.; He, H.; Liu, T.; Benny, P.; Bryan, J. N.; Berkman, C. E. A phosphoramidate-based prostate-specific membrane antigen-targeted SPECT agent. *Prostate* **2012**, *72*, 904−912.
(56) Liu, T.; Wu, L. Y.; Choi, J. K.; Berkman, C. E. Targeted photodynamic therapy for prostate cancer: inducing apoptosis via activation of the caspase-8/−3 cascade pathway. *Int. J. Oncol.* **2010**, *36*, 777−784.
(57) Bergers, G.; Benjamin, L. E. Tumorigenesis and the angiogenic switch. *Nat. Rev. Cancer* **2003**, *3*, 401−410.
(58) Jain, R. K. Normalization of tumor vasculature: an emerging concept in antiangiogenic therapy. *Science* **2005**, *307*, 58−62.
(59) Helmlinger, G.; Yuan, F.; Dellian, M.; Jain, R. K. Interstitial pH and pO2 gradients in solid tumors in vivo: high-resolution measurements reveal a lack of correlation. *Nat. Med.* **1997**, *3*, 177−182.
(60) Jain, R. K. Barriers to drug delivery in solid tumors. *Sci. Am.* **1994**, *271*, 58−65.
(61) Staudacher, A. H.; Brown, M. P. Antibody drug conjugates and bystander killing: is antigen-dependent internalisation required? *Br. J. Cancer* **2017**, *117*, 1736−1742.
(62) Ley, C. R.; Beattie, N. R.; Dannoon, S.; Regan, M.; VanBrocklin, H.; Berkman, C. E. Synthesis and evaluation of constrained phosphoramidate inhibitors of prostate-specific membrane antigen. *Bioorg. Med. Chem. Lett.* **2015**, *25*, 2536−2539.

https://doi.org/10.1021/acs.bioconjchem.1c00435
Bioconjugate Chem. 2021, 32, 2386−2396